THE ASTROPHYSICAL JOURNAL, 478:435–445, 1997 April 1

THE FATE OF CANNIBALIZED FUNDAMENTAL-PLANE ELLIPTICAL GALAXIES

MARTIN D. WEINBERG[1]
Department of Physics and Astronomy, University of Massachusetts, Amherst, MA 01003-4525; weinberg@phast.umass.edu
Received 1996 July 19; accepted 1996 October 24

ABSTRACT

Evolution and disruption of galaxies orbiting in the gravitational field of a larger cluster galaxy are driven by three coupled mechanisms: (1) tidal heating due to its time-dependent motion in the primary; (2) mass loss due to the tidal strain field; and (3) orbital decay. Previous work demonstrated that tidal heating is effective well inside the impulse approximation limit. Not only does the overall energy increase over previous predictions, but the work is done deep inside the secondary galaxy, e.g., at or inside the half-mass radius in most cases. Here these ideas applied to cannibalization of elliptical galaxies with fundamental-plane parameters.

In summary, satellites with masses between 0.1% and 10% of a cluster giant are evaporated or significantly evolved by internal heating as they sink to the center. This suggests that long-lived merger-produced multiple nuclei giants should be rare. The precise location of the survival-evaporation boundary and the central concentration of the stripped-mass profile depend on the rate of orbital decay. Large secondaries evaporate preferentially, provided the orbital decay takes place over roughly five or more orbits. We estimate that secondaries with mass ratios as small as 1% on any initial orbit evaporate, and those on eccentric orbits with mass ratios as small as 0.1% evolve significantly and nearly evaporate in a galactic age. Captured satellites with mass ratios smaller than roughly 1% have insufficient time to decay to the center. After many accretion events, the model predicts that the merged system has a profile similar to that of the original primary with a weak increase in concentration.

Subject headings: celestial mechanics, stellar dynamics — galaxies: evolution — galaxies: interactions — galaxies: kinematics and dynamics

1. INTRODUCTION

The current picture of galaxy evolution in clusters leads naturally to galactic cannibalism, especially deep in the potential well where the giants reside. Although multiple nuclei candidates have been identified (e.g., Tonry 1985; Lauer 1988), recent searches turned up many fewer inner core objects than expected (S. Tremaine 1995, private communication).

A closer look at the evolutionary picture is motivated by the recent demonstration that heating of galaxies or star clusters because of the time-dependent tidal field can drive their evolution at a rate beyond impulse approximation estimates (Weinberg 1994a, 1994b, and 1994c, hereafter W1, W2, and W3, respectively; Murali & Weinberg 1996a and 1996b, hereafter MW1 and MW2, respectively). This theory invalidates the following often used argument. The higher density of satellite galaxies implies shorter internal orbital times than the orbit of the satellite itself. Therefore, the stellar orbits in the satellite will be adiabatically invariant to the tidal force, and since the dynamical friction timescale is much less than a Hubble time for galaxy masses above $10^9\ M_\odot$, the satellite should sink to the center without suffering tidal disruption and remain a distinct compact entity. This paper presents estimates of the evolutionary path and evaporation lifetime for the cannibalized fundamental-plane elliptical galaxies. We will find that ellipticals with sufficient mass to decay are heated and evaporated before a multiple nucleus system can result, although such systems may exist transiently. The results also illustrate the interplay between tidal heating, tidal stripping, and orbital decay. For example, if the sinking is very rapid, the integrated work done by tidal heating can be too small for significant evaporation. Nonetheless, the likely evaporation of accreted galaxies with masses varying over several orders of magnitude in the fundamental plane may help reconcile the observation of a bimodal velocity distribution of multiple nuclei (Tonry 1985) as a dynamical friction–mediated selection effect (Merritt 1984) and/or a transient population of evaporating secondaries.

We begin with a description of the astronomical scenario in § 2. All members of the fundamental plane are represented by a spherical model with fixed initial concentration; this is roughly consistent with the observed fundamental-plane relations given the Faber-Jackson (1976) relation, although the best estimates suggest a weak dependence on concentration. We assume that the secondary is captured from the cluster by dynamical drag, and we consider evolution after the secondary is bound to the primary. The important dynamical ingredients and their implementation are briefly discussed in § 3; the technical details can be found in Appendices A and B and elsewhere (W2; MW2). The results for a number of astronomical scenarios are described in § 4; these include survival and evolution as a function of mass, orbital decay, and the resulting distribution of stripped stars in the primary. We compare them with the published *n*-body work and discuss the sensitivity of the results to the intrinsic dynamical approximations at the end of this section. A summary is presented in § 5.

2. ASTRONOMICAL SCENARIO

2.1. *Background Profile and Fundamental-Plane Scaling*

I have chosen a King model for both the primary and the secondary. King models with $\log c = 2.35$ are representative elliptical profiles (e.g., Mihalas & Binney 1981; Vader & Chaboyer 1994), although King models are not good fits in

[1] Alfred P. Sloan Foundation Fellow.

all cases.[2] Nonetheless, the mass model parameterizes the range of stellar orbital times, and this range determines the overall evolution rate from the resonant heating process, to be described below. An appropriate concentration ensures that a realistic range of orbital timescales are included. The conclusions are weakly dependent on the inner profile and other structural details of the model for high concentration (see § 4.4.4).

The radius and mass concentration is chosen according to two fundamental-plane relations. The first is based on the virial theorem and the Faber-Jackson relation, $L \propto \sigma^4$ (Faber & Jackson 1976), which results in the following scaling:

$$R \propto M^{1/2} \tag{1}$$

and $\rho \propto M^{-1/2}$. The concentration parameter is invariant under any fundamental-plane scaling that also assumes the Faber-Jackson relation. Therefore, all three King model parameters, mass, tidal or maximum radius, and concentration, are fixed for each secondary of given mass. The second is based on recent observed fundamental-plane relations (e.g., Pahre, Djorgovski, & de Carvalho 1995; S. M. Faber 1995, private communication):

$$R \propto M^{0.9} \, . \tag{2}$$

To reduce the overall number of parameters in this study, I have chosen to retain the constant-concentration models, even though recent fundamental relations predict that central density, and therefore concentration class, scales with mass. Changes in concentration predominantly change the inner profile and, as noted, only weakly affect the overall evolutionary track of the accreted secondary.

There are three remaining parameters: orbital energy, orbital eccentricity, and a secondary-to-primary mass ratio. Orbital evolution is determined using local dynamical friction that requires the secondary to be inside the primary (see §§ 3.4 and 4.4.3). The initial orbits for the secondaries, then, are chosen to have an energy whose circular orbit encloses 99% of the primary mass. In other words, we consider evolution just subsequent to capture. Eccentricity is parameterized by the ratio of orbital angular momentum to the maximum defined by the energy of the orbit, $\kappa \equiv J/J_{\max}(E)$, and five values are chosen: 0.1(0.2)0.9. A pure circular (radial) orbit has $\kappa = 1.0$ ($\kappa = 0.0$). Because a captured elliptical is likely to be on a plunging orbit, we will emphasize the $\kappa = 0.1$ case. A parabolic encounter would have a larger value of κ. The model profile and location of initial orbits in the model are shown in Figure 1. Finally, each set of five orbits is evolved for four different secondary-to-primary mass ratios: 10^{-4}, 10^{-3}, 10^{-2}, and 10^{-1}.

Dimensionless units are chosen for the King model such that $G = M = 1$ and total gravitational potential energy $W = -1/2$. For the $W_0 = 9.5$ King model, $R_{\rm core} = 0.5$ with outer radius $R_{\max} = 7.91$ in these units. I will take a fiducial central cluster galaxy to have $M = 10^{14}\ M_\odot$ inside of $R_{\max} = 300$ kpc, which sets the timescale quoted in years in § 4. This fiducial choice is similar to that for M87 (e.g., Binney & Tremaine 1987; Merritt & Tremblay 1993). A different choice simply shifts the quoted timescale by the ratio

$$\frac{T}{T_0} = \left(\frac{M}{10^{14}\ M_\odot}\right)^{-1/2} \left(\frac{R_{\max}}{300\ \text{kpc}}\right)^{3/2} . \tag{3}$$

For reference, orbital periods for the fiducial scaling whose guiding center radii enclose 10%(20%)90% for $\kappa = 0.1(0.2)0.9$ are described in Figure 2.

[2] The concentration parameter is defined as $\log c \equiv \log_{10} (R_{\max}/R_{\rm core})$.

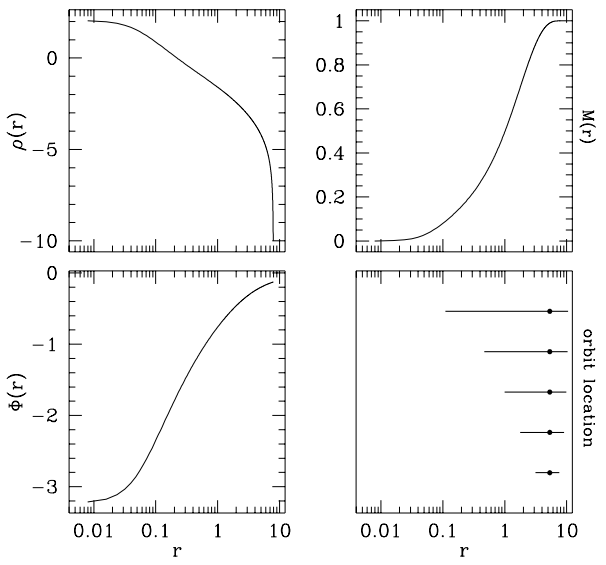

FIG. 1.—Density, mass, and potential for $W_0 = 9.5$ King model in dimensionless units. The model is nearly isothermal for $0.05 \lesssim r \lesssim 5$. The lower right panel shows the pericenter and apocenter radii for each orbit (ends of segments) and guiding center (circular orbit) radii (*solid dots*).

3. METHOD OVERVIEW

Evolution in the cannibalized ellipticals is caused by the following four interacting physical effects: (1) resonant heating and orbit shocking; (2) self-consistent gravity; (3)

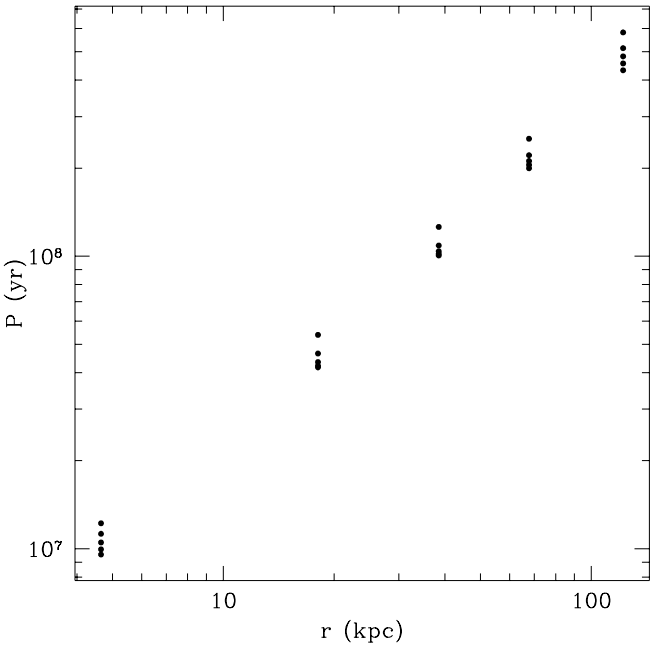

FIG. 2.—Periods of orbit scaled to a central cluster galaxy with $M = 10^{14}\ M_\odot$ and $R_{\max} = 300$ kpc. The dots represent the orbital periods with the guiding center radius enclosing 10%(20%)90% of the primary mass. The values $\kappa = 0.1(0.2)0.9$ are ordered from bottom to top.

tidal stripping; and (4) dynamical friction. These will be briefly described below, with additional detail in Appendices A and B. We will see that dependencies in the effect of the four physical processes govern the subsequent evolution.

3.1. *Resonant Heating*

The orbiting secondary galaxy experiences a differential or *tidal* force. The combined strain and compressive force are time-dependent and can do work on the secondary galaxy. If the change in tidal force is rapid compared with internal orbital timescales, a *gravitational shock*, the work can be computed using the impulse approximation. However, even if the change in strain is slower than internal orbital timescales, significant work may still be done: most realistic galaxies will have resonances between the two (or more) internal orbital frequencies, the external forcing frequency that leads to significant energy and angular momentum exchange (W1; W2; W3).

More picturesquely, the time-dependent force will excite a wake in the secondary. The wake will be dominated by a quadrupole or barlike distortion whose pattern speed is determined by the external frequency. Similar to torquing by spiral arms, this "bar" then couples to the tidal force, transferring energy and angular momentum to resonant orbits. The perturbation theory–derived heating rates used here are in good agreement with n-body simulations (cf. MW2; Johnston, Hernquist, & Weinberg 1996), with the advantage of being able to follow a weak disturbance without noise.

3.2. *Self-Consistent Gravity*

By Jeans's theorem (e.g., Binney & Tremaine 1987), an equilibrium of regular orbits is described by a phase-space distribution function, $f = f(\boldsymbol{I})$, where the $\boldsymbol{I}$ are the actions (or energy and angular momentum for a spherical system). The associated potential and density solve the Poisson equation by construction. Although the actions of most orbits are invariant to the slowly changing tidal strain, the resonant heating described above changes the actions of some small subset of orbits, resulting in a slightly out of equilibrium system.

At regular intervals, the Poisson equation is solved iteratively to maintain equilibrium. Because the external force is assumed to do negligible work on an internal orbital timescale, all external perturbations may be temporarily turned off, which fixes the actions and simplifies the solution. So the overall evolution consists of two phases: (1) evolution of phase space due to external perturbations in a fixed gravitational potential and (2) dynamical readjustment with all perturbations removed. Practically speaking, a new equilibrium is only computed when the changing phase-space distribution implies a 1%–2% change to the density profile.

As the equilibrium profile evolves, new orbits become resonant with the external force. In this way, a small set of resonant orbits at any one time can change the global structure over a number of dynamical timescales. Finally, for the results below, the resulting equilibrium phase-space distribution is forced to be spherical and isotropic. This is not an in-principle demand—the numerical implementation is general—but a choice driven by available CPU time (see § 4.4.1).

3.3. *Tidal Stripping*

The outer boundary of a secondary is defined by the points at which a star is more strongly attracted by the primary. For a circular orbit, this point is the analogous inner Lagrangian point in the restricted three-body problem. However, for an eccentric orbit, this is not an easily parameterized problem; these points change as the secondary orbits, resulting in foliated stable and unstable regions (e.g., Keenan 1981). N-body simulations suggest that setting the boundary to the inner Lagrangian point at perigalacticon is a fair prescription.

The location of the inner Lagrangian point scales with the ratio of mean density of the secondary to mean density of the primary enclosed with the secondary's orbit. Therefore, as the secondary evolves because of time-dependent heating, as described in § 3.1, stars may find themselves on the unbound side of the tidal limit. This loss of material also changes the equilibrium. If too much material is evaporated, global equilibrium may be lost, and the smaller galaxy "disrupts."

3.4. *Dynamical Friction*

Finally, the orbit itself is evolving by dynamical friction. For small secondaries, Chandrasekhar's dynamical friction formula is an acceptable approximation (Chandrasekhar 1943; see, e.g., Binney & Tremaine 1987). This approximation assumes that the primary is infinite and homogeneous with the local value of density and distribution of velocities. The drag force is perpendicular to the motion of the secondary assuming velocity isotropy. For large secondaries, the situation is more complex (e.g., Hernquist & Weinberg 1989; Weinberg 1989), but the local approximation will be used for simplicity. Further consequences of the decaying orbit are an increasing resonant heating rate and a stronger tidal limit, both of which accelerate the evolution (see § 4.4.3 for further discussion).

4. EVOLUTION OF SATELLITE GALAXIES

The models and methods of §§ 2 and 3 are applied to groups of 20 models each. Each group of twenty has four mass ratios, $M_{\rm ratio} = 10^{-1}$, 10^{-2}, 10^{-3}, and 10^{-4}, and five eccentricities, $\kappa = 0.1(0.2)0.9$ (cf. Fig. 1). The two groups discussed here have guiding center orbits that enclose 99% of the primary mass. The first group uses the virial scaling, and the second uses the observed fundamental-plane scaling (cf. § 2).

Let us recall that the physical times quoted below assume a primary mass of $10^{14}\ M_\odot$ inside of 300 kpc. Equation (3) may be used to scale to any desired primary mass and radius.

4.1. *Disruption and Survival*

Figures 3, 4, 5, and 6 describe the mass evolution for fundamental-plane ellipticals as a function of initial eccentricity for the four mass ratios. The contours indicate the mass fraction remaining at the time indicated. The vertical axis shows increasing initial orbital eccentricity. Galaxies to the right of the 0.05 contour have completely evaporated. Heating and stripping is severe for the most eccentric orbits and the highest mass ratios. For the ratio 10^{-1}, the orbit decays in approximately ten orbits, and the galaxy has evaporated for all eccentricities by roughly 1 Gyr (Fig. 3). We will see in § 4.2 that evaporation occurs near the center of the host galaxy.

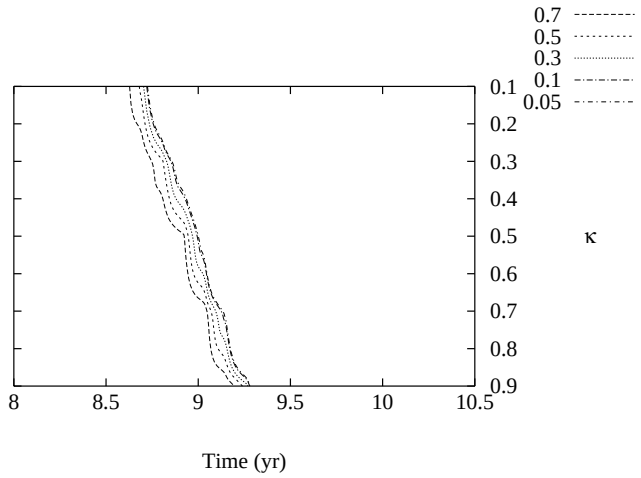

FIG. 3*a*

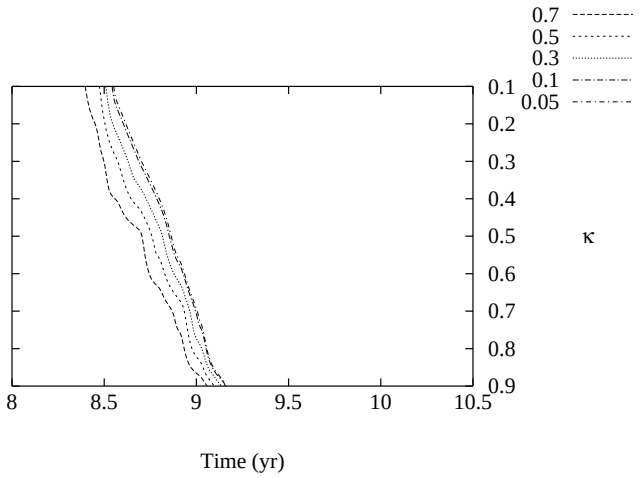

FIG. 3*b*

FIG. 3.—Contours show remaining mass fraction (key at upper left of each panel) as a function of time (logarithmic scale) and initial value of $\kappa = J/J_{\max}$. The secondary-to-primary mass ratio is 10^{-1}. (*a*) The virial fundamental-plane scaling. (*b*) The observed fundamental-plane scaling. The scalloping in the contours is caused by the projection of a finite grid.

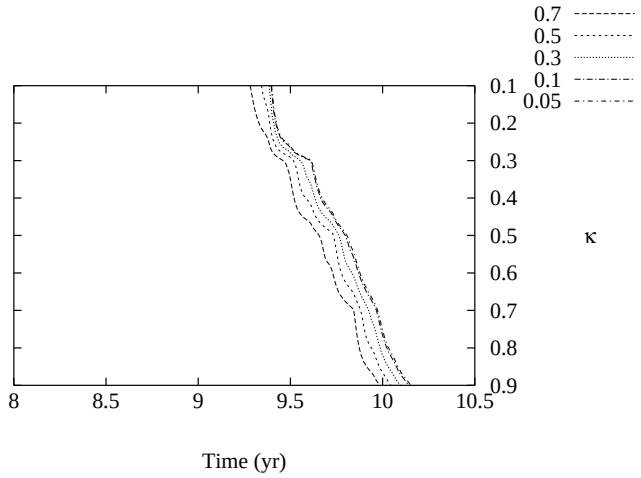

FIG. 4*a*

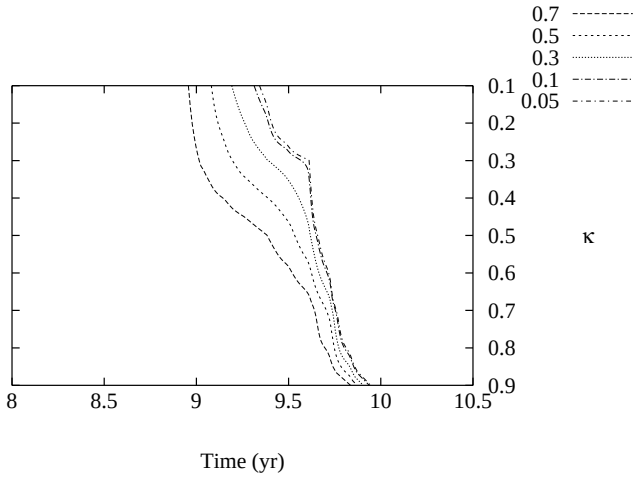

FIG. 4*b*

FIG. 4.—Same as Fig. 3, but for mass ratio 10^{-2}

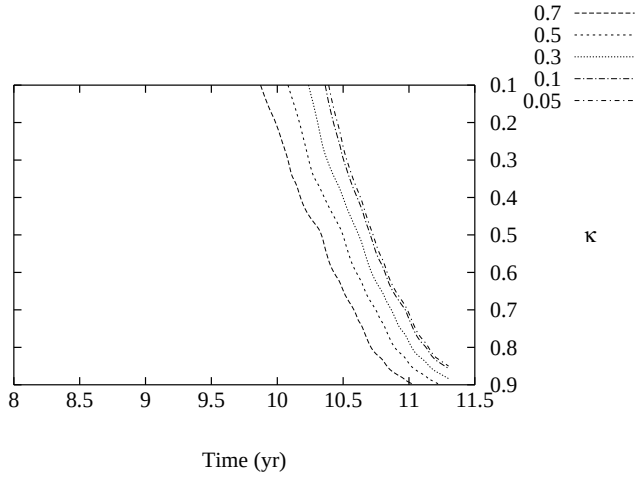

FIG. 5*a*

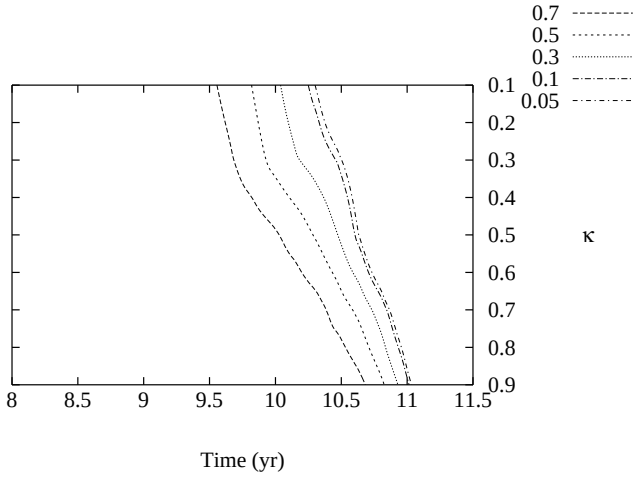

FIG. 5*b*

FIG. 5.—Same as Fig. 3, but for mass ratio 10^{-3}. The range in time is extended to accommodate alternative scalings.

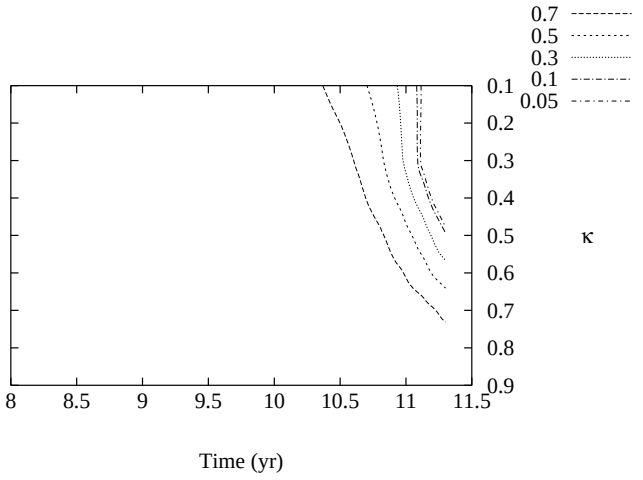

FIG. 6a

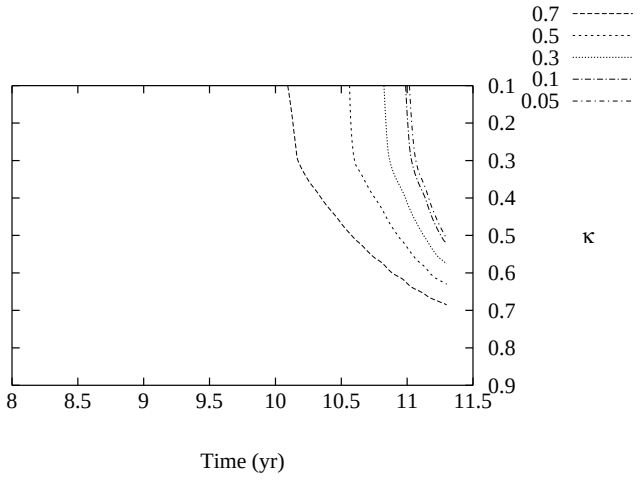

FIG. 6b

FIG. 6.—Same as Fig. 3, but for mass ratio 10^{-4}. The range in time is extended to accommodate alternative scalings.

The trends are similar for smaller mass ratios. A 1% secondary (Fig. 4) evaporates in 10 Gyr for a nearly circular orbit and in roughly 2 Gyr for an eccentric orbit. A 0.1% secondary—a large dwarf galaxy—does not completely evaporate in 10 Gyr even for an eccentric orbit, although it is close. Evolution is slower for smaller mass ratios because (1) the density of the secondary is larger and therefore couples more weakly to the tidal field, and (2) the orbital decay rate, which is proportional to the mass ratio, is slower.

4.2. *Orbital Decay*

Figure 7 shows the orbital evolution of initially $\kappa = 0.1$ orbits for the four mass ratios. The decay rate is computed using Chandrasekhar's formula with $\ln\Lambda = \max[\ln(R_{\rm circ}/r_{1/2}), 0.1]$, where $R_{\rm circ}$ is the radius of the guiding center for the secondary orbit and $r_{1/2}$ is the current half-mass radius of the secondary. Orbital torques are also computed in the local approximation with Chandrasekhar's formula. These eccentric orbits become more circular during their decay (Fig. 8), as previously described by Bontekoe & van Albada (1987). Initially, the $\kappa = 0.1$ orbits with guiding center trajectories enclosing 99% of the primary mass have apocenters outside the primary (cf. Fig. 1), which may lead to an overestimate of the decay time. For the fiducial model ($M = 10^{14}\ M_\odot$, $R_{\rm max} = 300$ kpc), only the 10% and 1% mass ratio secondaries can decay into the center in roughly 10 Gyr. The decay time for lower mass galaxies is increased by the concurrent mass loss.

The longer lifetimes for large initial κ are due to the lower stellar density in the path of the secondary and the proportionately longer decay times. For secondaries with $M_{\rm ratio} = 10^{-2}$ and $\kappa = 0.3(0.2)0.9$, the decay rate is nearly constant for orbits in the inner primary (roughly inside the half-mass radius of 60 kpc). The rate increases with decreasing initial eccentricity because the secondary spends a larger fraction of its time at higher primary density. This trend decreases the spread of decay times with eccentricity but does not compensate for the slower initial evolution of low-eccentricity orbits.

Similarly, the steep gradient in time across the mass contours in Figures 3–6 reflects the rapid mass evolution that takes place during the final stage of orbital decay. This trend is maintained at the smallest mass ratios, although full decay takes longer than a galactic age for the fiducial scaling.

Combining the results of this and the previous subsection, we reach the conclusion that *satellites that can fall to the center of a cluster giant by dynamical friction are evaporated by internal heating*. In all cases described, the decay occurs over at least ten orbits. Shorter decay times may not permit full evaporation.

4.3. *Distribution of Stripped Material*

As the secondary is stripped and evaporated, its stars preserve the instantaneous orbit and build up the primary, as suggested by Richstone (1976). The relative density distributions for secondaries on eccentric orbits, $\kappa = 0.1$, and the four mass ratios are shown in Figure 9.

The higher mass secondaries, $M_{\rm ratio} = 10^{-1}$ and 10^{-2}, lose mass quickly. Material is lost most quickly at pericenter, and individual episodes of mass loss during each orbit are visible in the outer galaxy. For $M_{\rm ratio} = 10^{-1}$, 90% of the mass is lost within the half-mass radius of the primary and 20% within 4 core radii. Overall, the remnant profile is steeper than the primary and could be a significant contributor to the inner light after a few such events. The two low-mass ratio cases, $M_{\rm ratio} = 10^{-3}$ and 10^{-4}, lose mass more gradually, and the distribution of stars lost in the outer primary is more extended than the primary, approximating a r^{-2} distribution. Both have guiding center radii larger than the primary half-mass radius and have lost roughly 80% and 50% of their total mass at the point depicted.

Overall, these results suggest that *mass evaporated from the secondary is distributed similarly to, and maybe steeper than, the profile of the primary*. After many accretion events, the merged profile will be slightly more concentrated.

4.4. *Comparison with Previous Work*

Recent work on dwarf-spiral galaxy mergers suggests that the distribution of stripped material depends on both the concentration of the secondary and the orbital decay time. Simulations by Walker, Mihos, & Hernquist (1996)

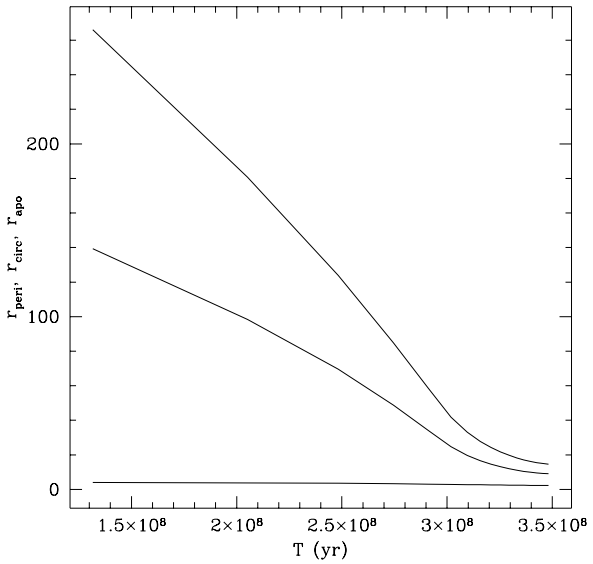

FIG. 7*a*

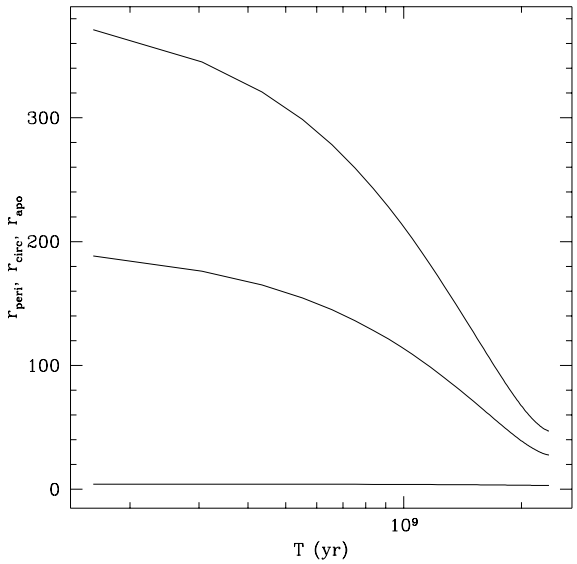

FIG. 7*b*

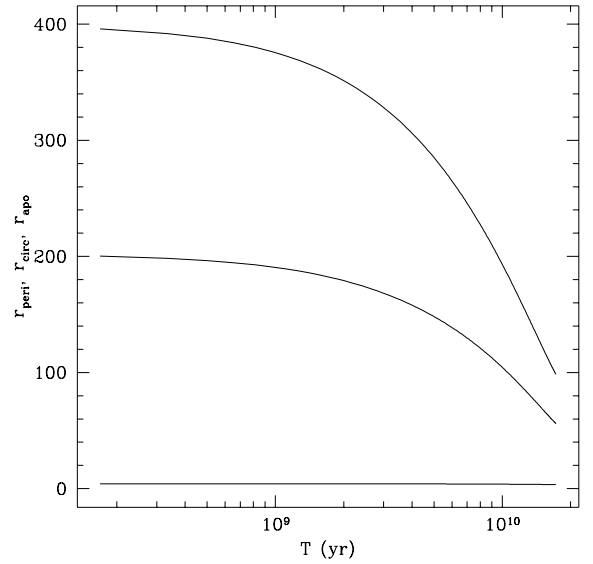

FIG. 7*c*

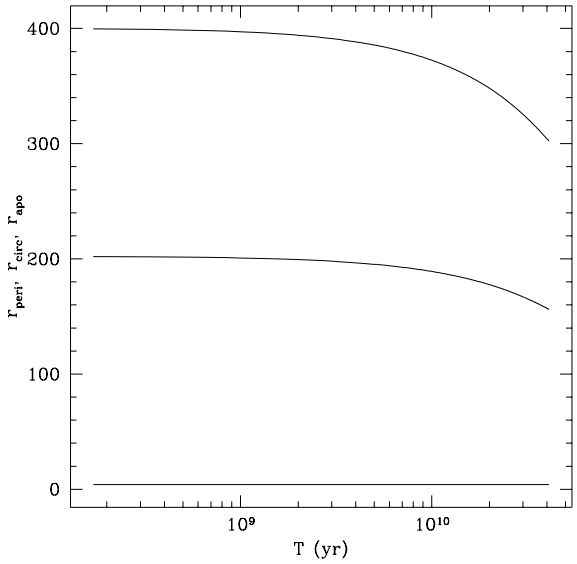

FIG. 7*d*

FIG. 7.—The orbital evolution for initial $\kappa = 0.1$ orbits for the four mass ratios 10^{-1}, 10^{-2}, 10^{-3}, and 10^{-4} (*right to left, top to bottom*) with observed fundamental-plane scaling (cf. Figs. 3–6). Satellites with $M_{\rm ratio} = 10^{-1}$ and 10^{-2} have zero mass at the final time shown.

show that a rapidly sinking satellite (infall in a few orbital times) is tidally stripped but can survive the accretion event. Simulations by Huang & Carlberg (1996) show the converse: the orbital decay takes many orbital times, during which the satellites are stripped and evaporated. Similarly, Quinn, Hernquist, & Fullagar (1993), who generalize the earlier work of Quinn & Goodman (1986), find that the secondary is completely stripped near the center, building up the inner regions by 10%–20%. The orbital decays take place over roughly six orbits. Considered together, these results suggest that survival or evaporation is correlated with sinking time. Based on the work here, these trends are expected: a larger infall rate reduces the integrated tidal work and the likelihood of evaporation.

Unfortunately, very little *n*-body work on merging self-consistent primary and secondary elliptical galaxies with masses differing by orders of magnitude has been reported. A search of the literature (G. D. Quinlan 1996, private communication) revealed one similar *n*-body study by Balcells & Quinn (1990, hereafter BQ), who performed simulations with $M_{\rm ratio} = 0.1, 0.2$ with rotating systems designed to explore the formation of counterrotating cores. The remainder of this section will discuss the inherent approximations in both the semianalytic and the *n*-body approaches, and compare this with the BQ result in particular.

Although the overall secondary evolution and distribution of stripped mass profiles described in §§ 4.1–4.3 are qualitatively similar to BQ, the resulting surface densities differ by an order of magnitude! Discrepancies between the two are likely to be caused by at least one of the following four features: (1) production of velocity anisotropies, (2) the validity of the perturbation approach for large secondaries, (3) different treatment of the orbital decay, and (4) differences in concentration and mass profiles. We discuss the sensitivity of our predictions to each of these below and

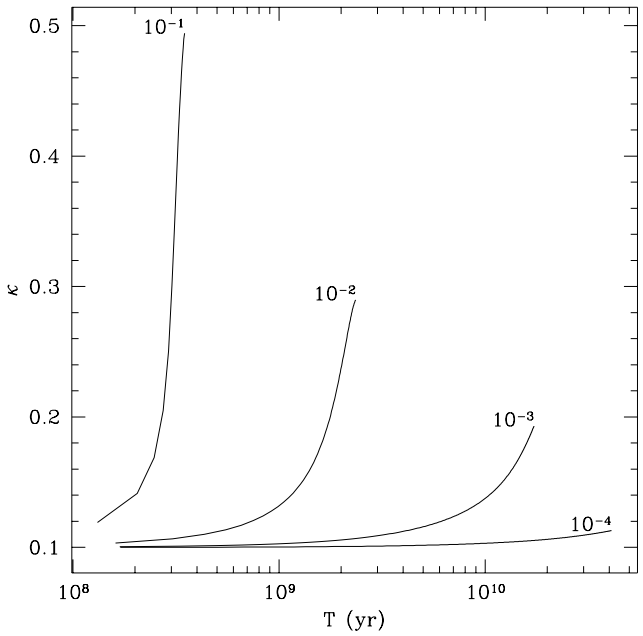

FIG. 8.—The change in $\kappa = J/J_{max}$ for mass ratios indicated for orbits with $\kappa = 0.1$ initially.

show that a plausible variance can resolve much of the discrepancy.

4.4.1. *Orbital Anisotropy*

For computational expediency, the computations described here do not follow the evolution of velocity anisotropies in the secondary. Instead, isotropy is enforced by assuming that the phase-space distribution is a function of energy alone, $f = f(E)$. This simplifies the solution of the Poisson equation for f, which is an integro-differential equation (e.g., Cohn 1979). The same iterative method is generalized straightforwardly to solve the spherical anisotropic case with $f = f(E, J)$ but is intensive computationally. Because the high-eccentricity stellar orbits will be preferentially lost, the isotropy assumption probably leads to an overestimate of the mass loss. MW2 (see their Fig. E1) compare the run of remnant mass with time for both an n-body simulation and the semianalytic approach used here. At early times, the agreement is excellent. At late times, the mass of the n-body remnant is larger than for the semianalytic simulation because of circular anisotropy, in addition to nonlinearity and relaxation.

4.4.2. *Perturbation Theory Limits*

It is difficult to assess precisely the limits of validity for the perturbation theory without a targeted study. However, direct comparison of this approach with n-body simulation at the phase-space level agrees extremely well for small-mass ratios (e.g., MW2; Johnston et al. 1996). For large secondaries, the $M_{ratio} \gtrsim 0.1$, the dynamical approximations made here will fail in the late stages of the accretion event. Near the center, the tidal radius of the secondary can be as large as the orbital radius, and the remnant mass can be as large as the primary mass enclosed within the orbital radius. This invalidates both the tidal force approximation and the local dynamical friction formula (see § 4.4.3). For this case, these final stages will be better described as a merger than a combination of orbital decay and tidally driven evaporation.

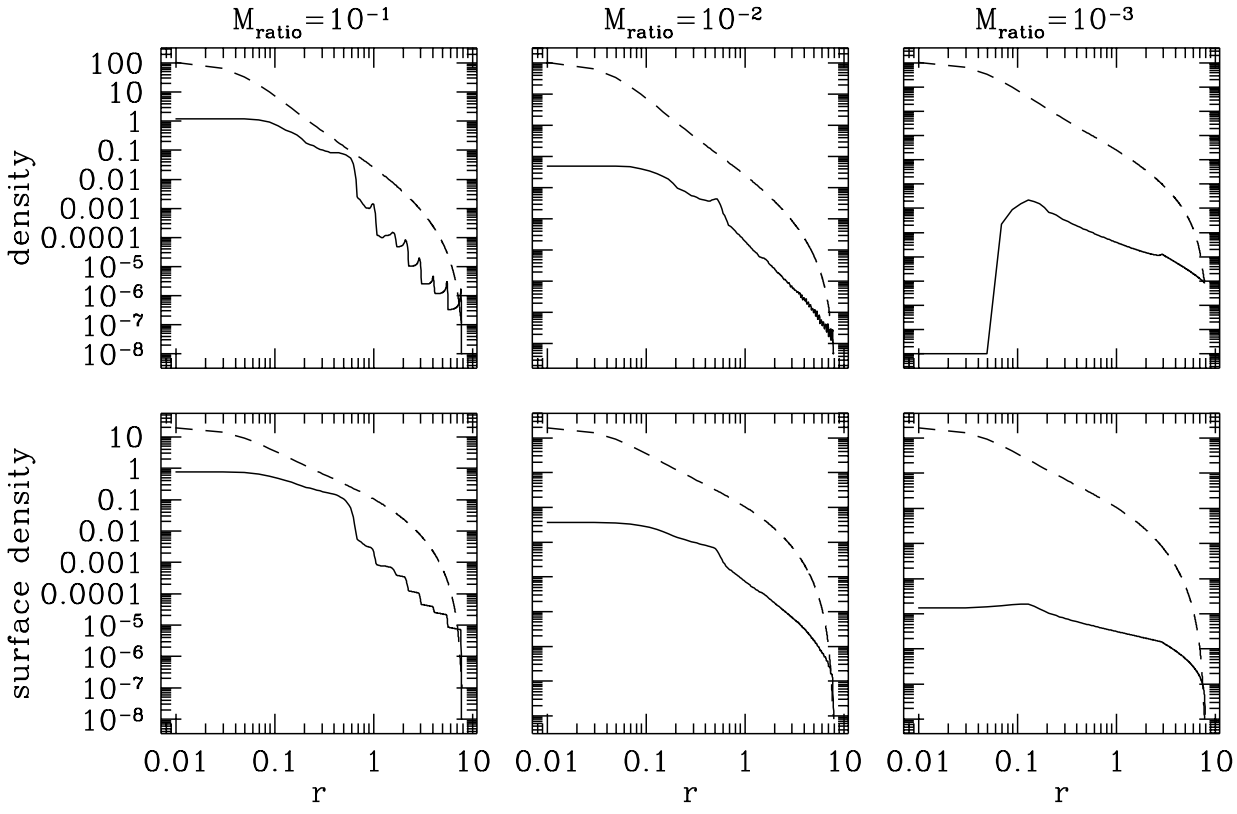

FIG. 9.—Distribution of stripped material from disrupting secondary (*solid curve*) compared with the background density (*dashed curve*) at three mass ratios (labeled). These use the virial scaling and dimensionless units (§ 2.1).

4.4.3. *Orbital Decay*

The orbital decay described in § 4.3 for $M_{\rm ratio} = 10^{-1}$ occurs over 10 orbits, with the largest fraction of the secondary evaporating in or near the core (cf. Fig. 9, *top left panel*). Orbital decay is more rapid in BQ, occuring over roughly three orbits. This and a previous discussion point toward orbital decay as a major part of the discrepancy. The orbital decay rate affects the secondary evolution in two ways. First, for a constant heating rate, the distribution of stripped material would be relatively extended for slow infall and centrally concentrated for rapid infall. Second, if the decay rate is rapid, the likelihood that the secondary survives infall to the center increases because the time-integrated tidal work on the secondary will be smaller. In reality, the heating increases toward the center, but overall the amount of material deposited in the center will increase as the decay time decreases. Survival or evaporation, then, depends on the orbital decay rate.

Chandrasekhar's dynamical friction formula (cf. § 3.4) treats the primary galaxy as an infinite homogeneous medium and will only be accurate for very small secondaries. The overall response of the primary *will* be important for large secondaries (e.g., Weinberg 1989). In addition, the local dynamical friction formula will overestimate the decay rate for a small remnant orbiting in the core. These problems may suggest using n-body methods exclusively, but n-body simulations do not resolve this issue easily. Simulations with too few particles overestimate the merger times because noise acts to amplify drag (e.g., Leeuwin & Combes 1996). Clearly, this subject requires further work.

Nonetheless, we may explore the effects of different decay rates with the semianalytic machinery. Figure 10 describes the distribution of stripped material for decay rates increased successively by a multiplicative factor. The softened Jaffe profile used by BQ is similar to a $W_0 = 6.5$ King model, and their orbit has $\kappa \approx 0.5$. The run in the left panels in the figure have the the fiducial form of ln Λ, and those in center and right panels have ln Λ increased by factors of 1.5 and 2, respectively. For the default value of ln Λ, the secondary disrupts outside the core. By increasing ln Λ by a factor of 1.5, the decrease in decay time allows the secondary to nearly reach the core before disrupting. By increasing ln Λ by a factor of 2, the secondary reaches the core before disrupting and joins the secondary distribution. The resulting profile with enhanced dynamical friction is similar to Figure 10 in BQ, although the semianalytic results underproduce the central buildup. The orbital decay rate in the $2 \times \ln \Lambda$ case is comparable to that of BQ. However, the details of the profile inside the core radius are not reliable because the dynamics of the merging are not taken in account.

4.4.4. *Central Concentration*

Figure 11 shows the space density of stripped material relative to the background profile for King models with $W_0 = 6$–11 and the singular isothermal sphere (labeled $W_0 = \infty$). As in § 4.3, the primary and secondary have the same profile initially. The accreted galaxies have 1% of the primary mass and $\kappa = 0.1$ initially. The choice of $M_{\rm ratio} = 10^{-2}$ helps ensure the validity of the perturbation approach. As in previous figures, the results are not phase-averaged, and distinct features in these profiles are due to particular orbits. For the highest and lowest mass concentrations, the singular isothermal and $W_0 = 6$ cases, the accreted galaxy survives and settles at the center with roughly 10% and

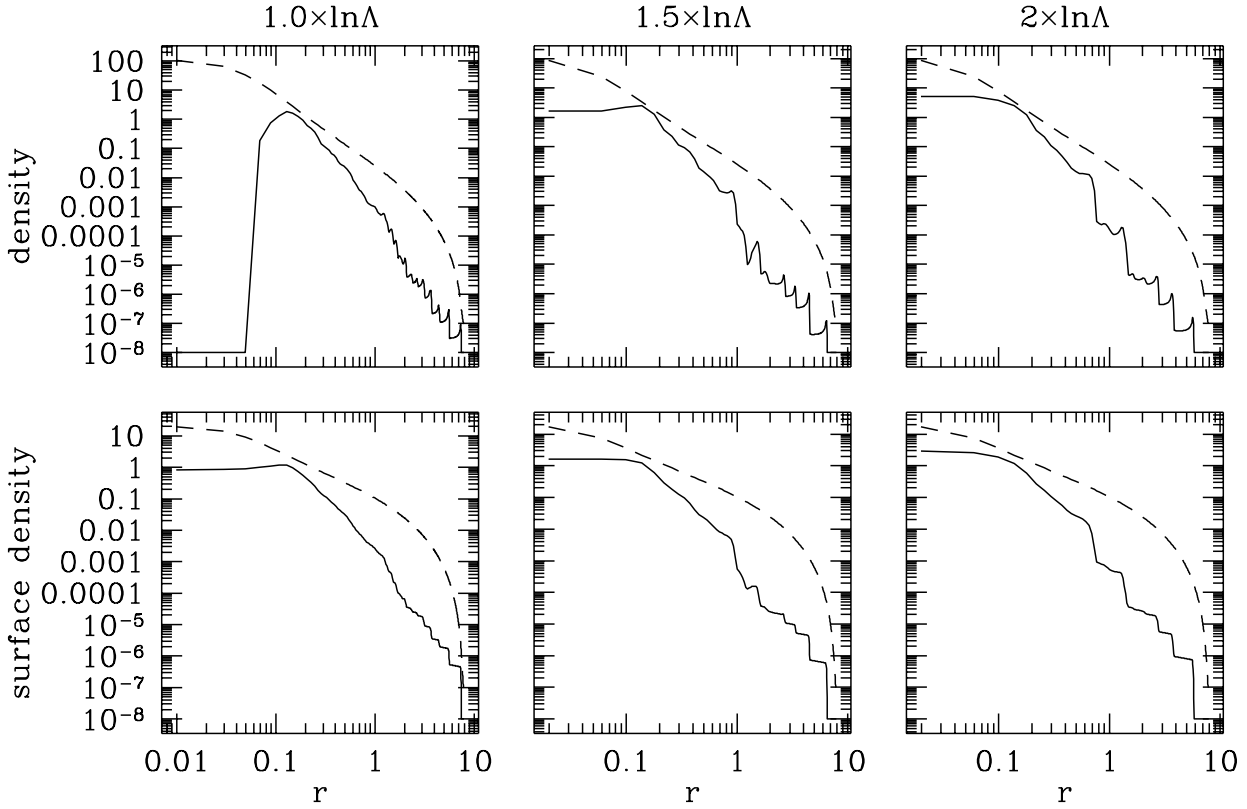

FIG. 10.—Distribution of stripped material for a $W_0 = 6.5$ King model family with $\kappa = 0.5$ and $M = 0.1$ for comparison with BQ. The values of ln Λ that are larger than the fiducial value by a factor of 1 are shown.

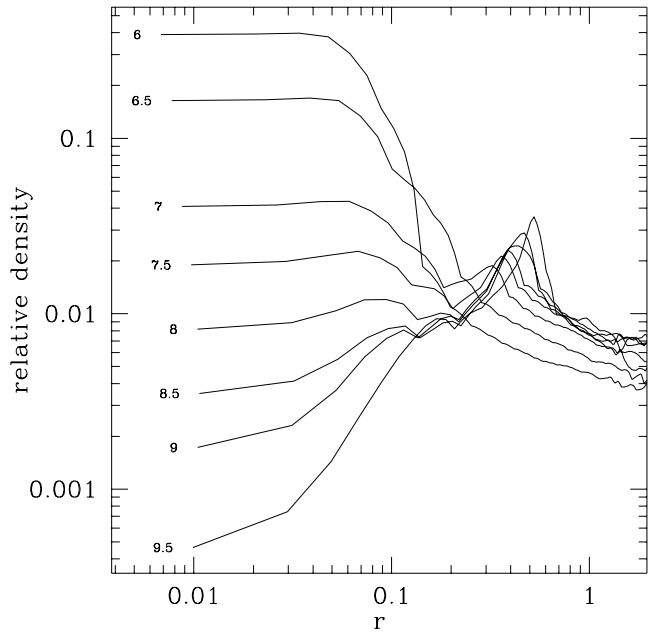

FIG. 11*a*

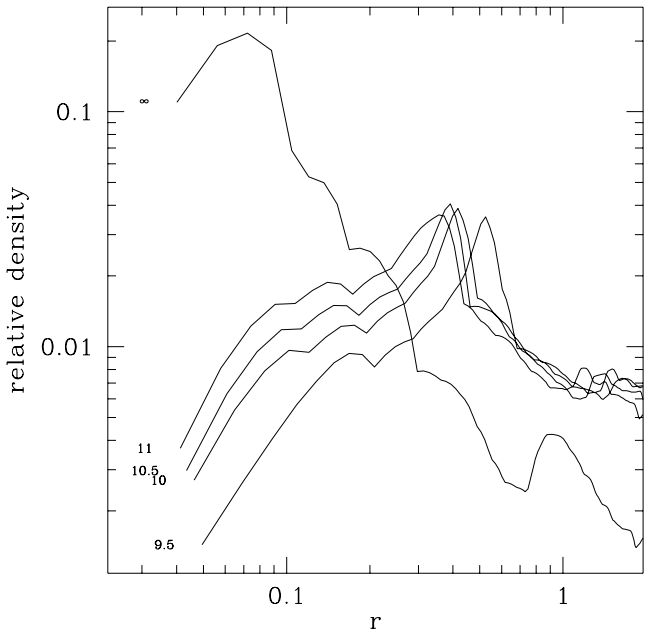

FIG. 11*b*

FIG. 11.—Distribution of stripped material for profiles relative to the background for different central concentrations (label at left)

20% remaining, respectively. The profiles in Figure 11 do not include the mass of the survivor. In all other cases, evaporation occurs near the center. For low-concentration galaxies (Fig. 11*a*), the relative density of the stripped material increases toward the center. For $W_0 \gtrsim 7$, the secondary is evaporated before reaching the core and produces a peak in the relative density at that point. The heating outside the core increases with concentration. The run of relative density is similar for King models with $W_0 \gtrsim 9.5$. The peak relative density of 40% for the $W_0 = 6$ case is remarkable considering the 1% initial mass ratio. The stripped-mass profile for the singular isothermal sphere is more centrally concentrated and, with a peak relative density of 20%, nearly an order of magnitude higher than the $W_0 = 11$ case.

In summary, the trends with concentration reveal a complicated interplay between the details of the profile and the heating rate, preventing generalization. The profile determines both the orbital decay of the secondary and the frequencies of the perturbing tide on the stellar orbits of the secondary. Surprisingly, the low-concentration King models are less subject to tidal evaporation. The evaporation rate for the core-free singular isothermal model is lower than the King models at large radii and much higher at small radii. It is not clear whether or not other cuspy profiles will follow suit.

5. SUMMARY

The major conclusions of this work are as follows:

1. Time-dependent heating can evaporate secondaries with mass ratios as small as 1% within a galactic age. Satellites that can fall to the center of a cluster giant by dynamical friction are evaporated by tidal heating in the process, provided they do not fall too quickly (e.g., in fewer than roughly five orbits). The boundary between survival and evaporation will depend on the orbital decay rate. The difference with the naive prediction that the denser satellite galaxies will invariably survive orbital decay is due to the breakdown of the one-dimensional adiabatic invariant in three-dimensional stellar systems, as described in MW1.

2. Secondaries with mass ratios as small as 0.1% on eccentric orbits are significantly evolved and nearly evaporated. Because capture by dynamical drag will preferentially produce high-eccentricity companions, this predicts a lower limit: captured secondaries with mass smaller than 0.1% of the primary will survive.

3. The profile of the mass loss as the satellite decays is similar to, but slightly more concentrated than, that of the original primary. This implies that the concentration of the cluster giant will increase gradually after many mergers.

4. Evaporation occurs near the center of the primary; material from both cores combine into a single entity. This suggests that long-lived multiple nuclei giants should be rare. Of course, the accretion event will appear as a multiple nucleus system over the final few orbits. This scenario does not address the possibility that a massive accretion event will lead to a nuclear gas accretion and a burst of star formation (Hernquist & Mihos 1995), and perhaps form a second nucleus in situ.

5. The details of the evolution depend intimately on stellar orbits in both the primary (through dynamical friction) and the secondary (through tidal heating). This is a complicated multiscale problem. The semianalytic approach treats the orbital dynamics accurately but fails in the late stages of evolution when nonlinear interaction is important. The *n*-body approach gives insight into the late stages of merger-dominated evolution, but accurate resolution of the orbital dynamics is challenged by particle "noise." This motivates a combined approach for future work.

I thank Sandy Faber, Chris Mihos, Chigurupati Murali, Gerry Quinlan, Doug Richstone, and Scott Tremaine for comments and suggestions. This work was supported in part by NASA grants NAGW-2224 and NAG 5-2873, and the Sloan Foundation.

APPENDIX A

ORBIT SHOCKING

Shocking caused by an oscillatory perturbation is a straightforward variant and is somewhat easier to compute than a one-shot adiabatic disturbance described in W2. For example, if a cluster is dynamically part of the thick disk, then the perturbation has the form $V_p = g(t)z^2$, where $g(t)$ is then a periodic function of time. The function $g(t)$ may be expanded as a Fourier series in its vertical oscillation period, P:

$$g(t) = \sum_{k=-\infty}^{\infty} g_k e^{ik\omega t} , \tag{A1}$$

where $\omega = 2\pi/P$ and

$$g_k = \frac{1}{P}\int_0^P dt g(t) e^{-ik\omega t} . \tag{A2}$$

The Laplace transform of this Fourier series is trivial and is

$$\hat{g} = \sum_{k=-\infty}^{\infty} \frac{g_k}{s - ik\omega} . \tag{A3}$$

For physical scenarios (e.g., smooth and continuous mass profiles), g_k will converge rapidly with increasing $|k|$. The time-dependent perturbation theory is not sensitive to and does not require frequency stability over many orbital periods. A slow drift due to orbital decay or a wobble due to nonaxisymmetric perturbations will only broaden the frequency distribution of the resonance. The effect on the system will be negligible as long as the frequency breadth is small compared with the stellar orbital frequencies. The calculation is analogous for orbit shocking with the following changes:

1. The potential perturbation expansion will be more general than the z^2 dependence and will include all second-order moments (all Y_{2m} terms).
2. The Fourier expansion of $g(t)$ will have two indices corresponding to the radial and azimuthal periods of the cluster orbit.

See MW2 for details.

We are only interested in the long-term secular change in the distribution function, after any transients have decayed. Following W2, we Fourier and Laplace transform the perturbed Boltzmann equation. The secular contribution is second order in the distribution function, and the inverse Laplace transform leads to the desired result. As mentioned above, any slow variation in the function $g(t)$, e.g., due to the initial conditions or the evolution itself, has little effect on the secular change that allows one to eliminate the temporal details altogether (MW2). Alternatively, one can choose a convenient form for the long-term behavior $g(t)$, such as a square pulse, and perform the transforms explicitly. Either way, for timescales that are large compared with the stellar orbital times, the secular change due to heating becomes

$$\frac{df_2}{dt} = \pi \sum_{k,\boldsymbol{l}} |g_k|^2 \boldsymbol{l} \cdot \frac{\partial}{\partial \boldsymbol{I}} (V_{\boldsymbol{l}} V_{-\boldsymbol{l}}) \boldsymbol{l} \cdot \frac{\partial f_0}{\partial \boldsymbol{I}} \delta(k\omega + \boldsymbol{l} \cdot \Omega) ,$$

where $V_{\boldsymbol{l}}$ denotes the action-angle transform of the tidal potential. As described in MW2, this expression has the form

$$\frac{\partial f}{\partial t} = \frac{df_2}{dt} = \frac{\partial}{\partial E}\left[A(E)\frac{\partial f}{\partial E}\right], \tag{A4}$$

which may be solved by standard techniques (e.g., Crank-Nicholson or Chang-Cooper 1970 schemes).

A paper in preparation will describe the effects of disk shocking, orbit shocking and thick-disk shocking on the galactic population of globular clusters.

APPENDIX B

TIDAL PERTURBATION

To compute the effect of an orbit in a galaxy, the galactic potential may be expanded in a frame that follows the cluster but is nonrotating. The force is

$$\boldsymbol{F}_t = -\nabla\Phi|_{R+r} + \nabla\Phi|_R , \tag{B1}$$

$$F_i \approx -\left|\sum_j \frac{\partial^2\Phi}{\partial x_i \partial x_j}\right|_{R=R(t)} x_j , \tag{B2}$$

where $\boldsymbol{R}$ describes the cluster, and $\boldsymbol{r}$ the position of a star relative to the cluster. The tidal potential then follows directly:

$$V_t = \frac{1}{2}\left|\left[\left(\frac{d^2\Phi}{dR^2} - \frac{1}{R}\frac{d\Phi}{dR}\right)\frac{(\boldsymbol{R}\cdot\boldsymbol{x})^2}{R^2} + \frac{1}{R}\frac{d\Phi}{dR}\,r^2\right]\right|_{\boldsymbol{R}=\boldsymbol{R}(t)}. \tag{B3}$$

Expanding equation (B3) in spherical harmonics, perturbed quantities may be computed as outlined in the Appendix A. The noninertial velocity-dependent forces are not easily incorporated into a potential and have been ignored here.

REFERENCES

Balcells, M., & Quinn, P. J. 1990, ApJ, 361, 381 (BQ)
Binney, J., & Tremaine, S. 1987, Galactic Dynamics (Princeton: Princeton Univ. Press)
Bontekoe, T. R., & van Albada, T. S. 1987, MNRAS, 224, 349
Chandrasekhar, S. 1943, ApJ, 97, 255
Chang, J. S., & Cooper, G. 1970, J. Comput. Phys., 6, 1
Cohn, H. 1979, ApJ, 234, 1036
Faber, S. M., & Jackson, R. E. 1976, ApJ, 204, 668
Hernquist, L., & Mihos, C. J. 1995, ApJ, 448, 41
Herquist, L., & Weinberg, M. D. 1989, MNRAS, 238, 407
Huang, S., & Carlberg, R. G. 1996, ApJ, submitted
Johnston, K. V., Hernquist, L., & Weinberg, M. D. 1996, in preparation
Keenan, D. W. 1981, A&A, 95, 334
Lauer, T. R. 1988, ApJ, 325, 49
Leeuwin, F., & Combes, F. 1996, MNRAS, submitted
Merritt, D. 1984, ApJ, 276, 26
Merritt, D., & Tremblay, B. 1993, AJ, 106, 2229
Mihalas, D., & Binney, J. 1981, Galactic Astronomy (2d ed.; San Francisco: Freeman)
Murali, C., & Weinberg, M. D. 1996a, MNRAS, submitted (http://xxx.lanl.gov/abs/astro-ph/9604049) (MW1)
———. 1996b, MNRAS, submitted (http://xxx.lanl.gov/abs/astro-ph/9602058) (MW2)
Pahre, M. A., Djorgovski, S. G., & de Carvalho, R. R. 1995, ApJ, 453, L17
Quinn, P. J., & Goodman, J. 1986, ApJ, 309, 472
Quinn, P. J., Hernquist, L., & Fullagar, D. P. 1993, ApJ, 403, 74
Richstone, D. O. 1976, ApJ, 204, 642
Tonry, J. L. 1985, AJ, 90, 2431
Vader, J. P., & Chaboyer, B. 1994, AJ, 108, 1209
Walker, I. R., Mihos, C. J., & Hernquist, L. 1996, ApJ, 460, 121
Weinberg, M. D. 1989, MNRAS, 239, 549
———. 1994a, AJ, 108, 1398 (W1)
———. 1994b, AJ, 108, 1403 (W2)
———. 1994c, AJ, 108, 1414 (W3)